RSC Advances

PAPER

View Article Online
View Journal | View Issue

Cite this: *RSC Adv.*, 2026, **16**, 13124

Electronic reactivity and drug binding in doped cycloparaphenylenes: toward multifunctional platforms for biosensing and targeted drug delivery

Noora B. Shwayyea,[a] Mustafa K. Salman,[a] Alaa M. Khudhair,[ab] Fouad N. Ajeel [ab] and Ali Ben Ahmed *[bc]

Cycloparaphenylenes (CPP) and their heteroatom-doped derivatives are emerging as interesting nanocarriers due to their adjustable electronic structures and π-conjugated frameworks. This study used density functional theory (DFT) to examine the structural, electrical, and adsorption characteristics of virgin CPP, nitrogen-doped CPP (N-CPP), and oxygen-doped CPP (O-CPP) in relation to two anticancer agents, hydroxyurea (HU) and thioguanine (TG). Geometry optimization verified the inherent stability of all carriers, whereas doping induced localized distortions that increased reactivity. Electronic tests indicated a consistent decrease in the energy gap after medication adsorption. HU functioned as a weak electron donor, resulting in little gap narrowing, whereas TG operated as a robust electron acceptor, causing substantial band-gap quenching-particularly in TG@O-CPP, where the gap practically disappeared, resulting in metallic-like behavior. Adsorption energies (−0.10 to −1.13 eV) and recovery periods revealed divergent kinetics: HU complexes desorbed almost quickly, while TG demonstrated more robust binding and extended residence lengths, especially on O-CPP. Charge-transfer research validated the contrasting donor–acceptor functions of HU and TG, supported by global reactivity indices indicating heightened electrophilicity and reduced hardness upon TG adsorption. The findings identify TG@O-CPP as the most promising system, with improved adsorption strength, substantial charge transfer, notable band-gap reduction, and adjustable electrical responsiveness. These results provide significant insights for the systematic design of CPP-based nanostructures in biosensing applications that need rapid reaction and in drug-delivery systems that require controlled release.

Received 6th December 2025
Accepted 20th February 2026

DOI: 10.1039/d5ra09445c

rsc.li/rsc-advances

1. Introduction

The World Health Organization reports that cancer continues to be one of the most prevalent causes of mortality worldwide, with nearly 10 million fatalities observed in 2025.[1] Genetic mutations, complex signalling dysregulations, and uncontrolled cellular proliferation are the causes of the disease, which results in tumor growth and metastasis.[2] Cancer continues to present substantial public health challenges as a result of its heterogeneity, tendency to develop drug resistance, and severe adverse effects associated with conventional chemotherapeutics, despite the extraordinary progress made in early detection and targeted therapies.[3] Additionally, chemotherapy and radiotherapy are frequently prescribed without regard to selectivity, which leads to systemic toxicity and diminished patient quality of life.[4] The imperative requirement for innovative strategies that can enhance therapeutic outcomes while minimizing adverse effects is underscored by these limitations.

Conventional anticancer therapies, while somewhat effective, often exhibit inadequate absorption, fast elimination, and insufficient tumor selectivity.[5] These disadvantages often result in systemic toxicity, multidrug resistance, and inadequate treatment results.[6] Nanomaterials have emerged as viable solutions to address these restrictions, owing to their distinctive physicochemical features, such as a high surface-to-volume ratio, adjustable size, and surface functionalization potential.[7] These characteristics enable nanocarriers to encapsulate hydrophobic or unstable pharmaceuticals, safeguard them from premature degradation, and promote regulated and prolonged release.[8] Nanoscale carriers may use the increased permeability and retention (EPR) effect in tumor tissues, resulting in preferential accumulation at the tumor location while preserving healthy tissues. These benefits render nanomaterials essential in the development of next-generation cancer treatments.

Cycloparaphenylenes (CPPs), also referred to as carbon nanohoops, have recently been identified as prospective host

[a]*Department of Physics, College of Science, University of Sumer, Iraq, Thi-Qar 64000, Iraq*

[b]*Department of Physic, College of Science, University of Sfax, Sfax 3000, Tunisia. E-mail: ali.benahmed@isbs.usf.tn*

[c]*Department of Biomedical, Higher Institute of Biotechnology of Sfax, University of Sfax, Sfax 3000, Tunisia*

materials for molecular encapsulation. This is a result of their well-defined internal cavities and cyclic π-conjugated frameworks.[9–11] In contrast to extended carbon nanostructures like graphene and carbon nanotubes, CPPs have atomically precise and monodisperse architectures that allow for predictable host–guest interactions and tunable electronic properties.[10,11]

Structural uniformity, controllable cavity size, and improved electronic responsiveness are among the numerous benefits that CPPs provide in comparison to traditional nanocarriers. Carbon nanotubes may suffer from aggregation and toxicity concerns, while graphene-based systems frequently experience structural heterogeneity. Soft carriers, including liposomes and polymeric nanoparticles, generally lack electronic tunability.[12,13] Nevertheless, CPP-based drug delivery systems are still in the early stages of development, facing obstacles such as the complexity of synthesis and the paucity of biological validation. Consequently, theoretical investigations are essential for comprehending adsorption mechanisms and directing rational design strategies, particularly through heteroatom doping to regulate electronic reactivity and drug-carrier interactions.

Hydroxyurea (HU) and thioguanine (TG) are the most widely recognized therapeutic agents for cancer treatment due to their demonstrated clinical efficacy. HU is an antineoplastic agent that has been approved for the treatment of chronic myeloid leukemia, sickle cell anemia, and some myeloproliferative disorders.[14] It predominantly achieves its pharmacological effect by inhibiting ribonucleotide reductase, which in turn reduces DNA synthesis and suppresses the uncontrolled proliferation of malignant cells.[15] While HU offers therapeutic advantages, its effectiveness is restricted by its non-specific distribution, brief plasma half-life, and dose-dependent cytotoxicity.[16] In contrast, TG is a purine analogue that is frequently used as an antimetabolite in the management of acute myeloid leukemia and other malignancies.[17] Ultimately, the drug induces apoptosis in quickly dividing tumor cells by causing cytotoxicity and disrupting nucleotide metabolism through its incorporation into DNA and RNA.[18] However, the therapeutic window of TG is limited by its low solubility, systemic toxicity, and rapid enzymatic degradation.[19] By incorporating HU and TG into nanocarrier systems, a promising approach is presented to improve tumor selectivity, prolong systemic circulation, and increase bioavailability, all while minimizing off-target toxicity.

In the last twenty years, the use of nanocarrier systems for drug administration has markedly increased, resulting in several advancements in cancer treatment. Initial research indicated that polymeric nanoparticles, liposomes, and dendrimers might augment the solubility and circulation duration of anticancer agents, hence improving treatment effectiveness relative to unencapsulated medicines.[20] Liposomal doxorubicin serves as a seminal instance of an FDA-approved nanomedicine, demonstrating decreased cardiotoxicity and enhanced pharmacokinetics compared to traditional doxorubicin.[21,22] Recent advancements have unveiled innovative carbon-based nanostructures, including graphene derivatives, and carbon nanotubes, which display distinctive π-conjugated topologies with promise for host–guest interactions and targeted delivery.[9] Functional changes, such as nitrogen- and oxygen-doping, have augmented the flexibility of CPPs, allowing better electrical characteristics, increased solubility, and selective interactions with medicinal compounds.[23] Concurrent advancements in stimulus-responsive nanocarriers, which may release medications in reaction to pH, temperature, or enzymatic stimuli, have emerged as effective solutions for precise and regulated administration.[8,24,25]

This work aims to construct and assess functionalized cycloparaphenylenes (CPPs), including nitrogen- and oxygen-doped variants, as nanocarrier systems for anticancer drug delivery. This study seeks to assess the potential of CPP-based frameworks to encapsulate and transport therapeutic compounds by examining their host–guest interactions, electrical characteristics, and structural changes, with a focus on enhancing stability, solubility, and tumor selectivity. The study aims to establish structure-property relationships governing drug-carrier binding through computational and theoretical analysis, thereby offering a rational foundation for the advancement of next-generation nanomedicine platforms that can address the limitations of conventional chemotherapy.

2. Computational details

First-principles calculations were implemented in this investigation to analyse the electronic properties and adsorption behavior of the systems under consideration. Utilizing the QuantumATK software package,[26] the Linear Combination of Atomic Orbitals (LCAO) method was employed to conduct structural optimization, energy calculations, and physicochemical characteristics. Molecular interactions were accurately modeled, and electronic properties were predicted with reliability through this method.

The Perdew–Burke–Ernzerhof (PBE) functional was implemented within the Generalized Gradient Approximation (GGA) to specify the exchange–correlation potential. Grimme's DFT-D3 correction scheme was implemented due to the critical function of van der Waals forces in adsorption processes.[27] Additionally, the application of PseudoDojo norm-conserving pseudopotentials in conjunction with GGA[28] guaranteed high accuracy while maintaining computational efficiency. The molecular dynamics protocols were also incorporated into the simulations to assess the thermodynamic stability of the optimized structures and to account for relaxation effects.

The pristine cycloparaphenylene (CPP) structure was selected as the reference system for the assessment of the impact of heteroatom contamination on drug-carrier interactions. Nitrogen- and oxygen-doped CPP models were generated through a substitutional methodology, which involved the substitution of one carbon atom in the CPP backbone with a nitrogen or oxygen atom, respectively. This substitution was implemented directly within the π-conjugated ring framework, while simultaneously maintaining the overall nanohoop architecture. All structures were completely optimized without symmetry constraints following the doping procedure to

facilitate complete structural relaxation and electronic redistribution. Doping was exclusively restricted to backbone substitution; no atoms were introduced into the internal cavity of CPP. With the use of pristine CPP as an internal reference system, this comparative framework facilitates a consistent theoretical evaluation of doping-induced effects.

Through established relationships, electronic parameters were determined. The energy gap (E_g) and Fermi level (E_{FL}) were determined by analyzing the lowest unoccupied molecular orbital (E_L) and the highest occupied molecular orbital (E_H).[29]

$$E_g = E_L - E_H \quad (1)$$

$$E_{FL} = \frac{E_H + E_L}{2} \quad (2)$$

The total energy difference was employed to calculate the adsorption energy (E_{ads}), a critical stability descriptor:[30]

$$E_{ads} = E_{complex\ structure} - (E_{substrate} + E_{anticancer\ drug}) \quad (3)$$

Koopmans' theorem-based equations were employed to derive global reactivity descriptors, including electronegativity (χ), chemical potential (μ), hardness (η), and softness (S). These descriptors are as follows:[31]

$$IP = -E_H \quad (4)$$

$$EA = -E_L \quad (5)$$

$$\eta = \frac{E_L - E_H}{2} \quad (6)$$

$$S = \frac{1}{2\eta} \quad (7)$$

$$\mu = \frac{E_L + E_H}{2} \quad (8)$$

$$\omega = \frac{\mu^2}{2\eta} \quad (9)$$

The work function (Φ), which denotes the minimum energy necessary for an electron to escape from the surface and enter the vacuum, was also calculated:[32]

$$\Phi = V_{el(+\infty)} - E_{FL} \quad (10)$$

(where $V\infty = 0$ is the reference point that is far from the surface).

$$\Delta\phi(\%) = \frac{\phi_b - \phi_a}{\phi_b} \times 100 \quad (11)$$

where the initial and final work functions, Φ_a and Φ_b, are denoted before and after the drug molecules are adsorbed onto the substrates, respectively.

Finally, transition state theory was employed to estimate the recovery time (τ), which is indicative of the desorption rate of adsorbed molecules:[33]

$$\tau = \frac{1}{\nu_0} e^{\frac{-E_{ads}}{k_B T}} \quad (12)$$

The attempt frequency is denoted by ν_0, Boltzmann's constant is denoted by k_B, and the absolute temperature is denoted by T.

The efficiency and reversibility of adsorption processes are directly correlated with this parameter, which is critically important in assessing the dynamic response of nanomaterials in drug delivery applications. Together, this computational protocol offers a dependable framework for comprehending adsorption phenomena, electronic modifications, and reactivity trends, thereby facilitating the rational design of nanocarriers for biomedical applications.

3. Result and discussion

3.1 Optimization structural

Fig. 1 displays the entirely optimized geometries of the pristine and doped cycloparaphenylenes (CPP, N-CPP, and O-CPP), as well as the anticancer medications hydroxyurea (HU) and thioguanine (TG). All carrier frameworks maintained their distinctive nanohoop symmetry during relaxation, which serves as confirmation of the CPP backbone's inherent thermodynamic stability. Substitution with nitrogen or oxygen atoms resulted in only localized perturbations of the π-conjugated ring. These distortions are anticipated to redistribute the electronic density and establish new active sites for adsorption. Concurrently, these subtle modifications emphasize the structural robustness of CPP and endow it with tunable host–guest properties.

Fig. 2 illustrates the optimized adsorption complexes. The HU and TG molecules formed stable physisorbed states by preferentially aligning near the dopant atoms or along the interior cavity of the nanohoop. The two pharmaceuticals exhibit significant differences when the shortest heavy-atom contacts are meticulously examined. HU exhibited moderate non-covalent stabilization, as evidenced by its adsorption

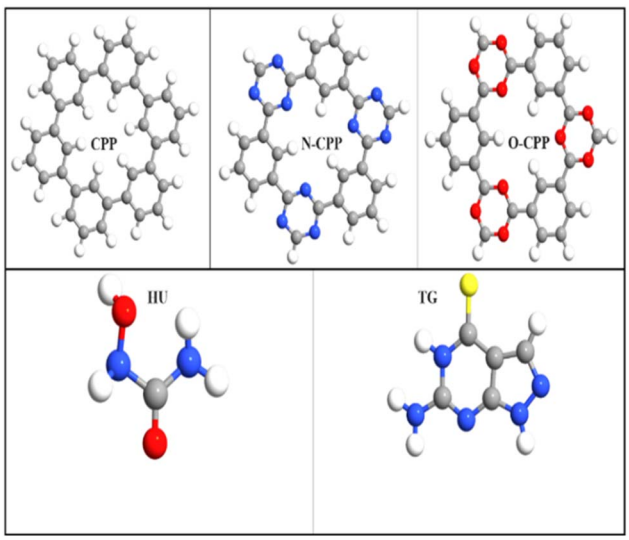

Fig. 1 Optimized geometries of the CPP, N-CPP, and O-CPP substrates, and HU and TG drugs.

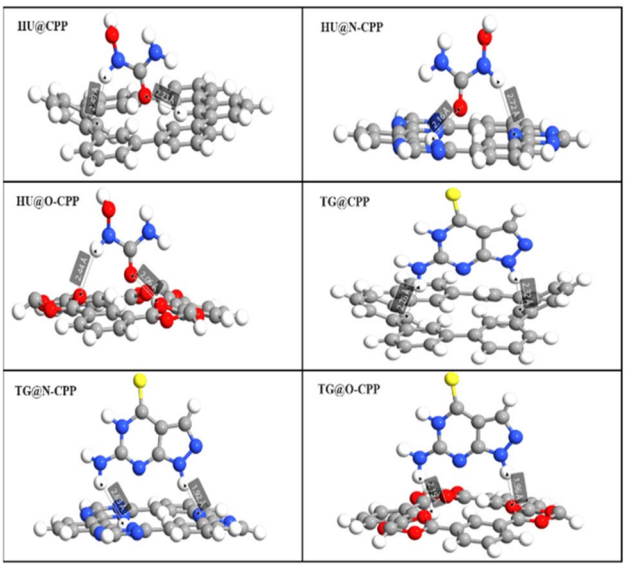

Fig. 2 Optimized geometries of the HU and TG drugs with CPP and doped derivatives.

Table 1 The shortest drug-carrier contact distances (Å) for optimized complexes, and charge transfer (Δq)

Structure	Shortest contact (Å)	Second contact (Å)	Δq (e)
HU@CPP	2.23	2.49	−0.177
HU@N-CPP	2.16	2.72	−0.109
HU@O-CPP	2.06	2.44	−0.154
TG@CPP	2.26	2.32	0.092
TG@N-CPP	1.92	2.63	0.141
TG@O-CPP	1.96	2.15	0.111

distances of 2.23–2.72 Å. On the other hand, TG exhibited the closest interactions with the carrier surface in the doped systems, with distances ranging from 1.92 to 2.63 Å. Specifically, TG@N-CPP and TG@O-CPP exhibited distances of approximately 1.9 to 2.0 Å. Table 1 summarizes the shortest heavy-atom contacts between the pharmaceuticals and the carrier frameworks, as extracted from the optimized geometries in Fig. 2. These values (1.9–2.7 Å) are within the typical physisorption regime and confirm the stronger stabilization of TG in comparison to HU, particularly in the doped systems.

Intriguingly, the local polarity of the framework was heightened by oxygen doping, resulting in shortened drug-carrier contacts for both HU and TG (approximately 2.0–2.4 Å). Conversely, nitrogen doping facilitated directional interactions that enhanced TG binding. The systematic reduction in intermolecular separation that occurs as a result of doping is directly correlated with the adsorption-energy hierarchy, which is summarized in Table 2. Doped systems exhibit a stronger binding than pristine CPP. Additionally, TG's extended residence time on the carrier surface and greater stabilization energy are structurally justified by its closer approach to HU.

In general, the structural optimization highlights the geometric adaptability of CPP-based frameworks and their ability to accommodate anticancer medications at separations that are conducive to efficient adsorption–desorption dynamics. A coherent structure-property relationship is established by the correlation between interatomic distances, adsorption energies, and dopant identity, which underpins the enhanced affinities of the N- and O-doped carriers. In the subsequent electronic analysis, the doping-induced modifications in band structure and density of states are thoroughly examined, based on these insights.

3.2 The electronic properties

The electronic behavior of the pristine and drug-loaded CPP frameworks was analyzed using the density of states (DOS) and band structures (Fig. 3–5), in conjunction with the frontier orbital energies summarized in Table 2.

Pristine CPP exhibited a well-defined semiconducting nature, with the HOMO and LUMO located at −6.87 eV and −3.82 eV, respectively, resulting in a band gap of 3.05 eV. The electronic configuration was only minimally perturbed by nitrogen doping, which resulted in a gap of 2.97 eV. Conversely, oxygen doping caused a more substantial reduction to 1.89 eV. The introduction of localized dopant states is responsible for the narrowing observed during doping, which enhances reactivity and compresses the frontier orbitals.

The DOS profiles exhibited modest perturbations upon HU adsorption, with HU@CPP and HU@N-CPP maintaining gaps that were close to the pristine frameworks (2.94 and 2.89 eV, respectively). This suggests that HU primarily interacts through mild physisorption, which is consistent with its larger drug-carrier distances. In contrast, the gap in HU@O-CPP was

Table 2 The values of the (E_T), Fermi level energy (E_{FL}), work function (Φ), E_{HOMO}, E_{LUMO}, and energy gap (E_g) for the structures in (eV) unit

Structure	E_T	E_{FL}	Φ	$\Delta\Phi$ (%)	E_H	E_L	E_g	ΔE_g(%)
CPP	−6048.426	−5.342	5.342	—	−6.865	−3.819	3.045	—
N-CPP	−6930.504	−6.851	6.851	28.29	−8.377	−5.409	2.968	−2.53
O-CPP	−8389.816	−5.870	5.870	9.89	−5.893	−4.005	1.888	−38.00
HU@CPP	−7682.943	−5.223	5.223	−2.23	−6.697	−3.756	2.941	−3.41
HU@N-CPP	−8564.448	−6.689	6.689	25.21	−8.163	−5.277	2.886	−5.23
HU@O-CPP	−10024.475	−5.780	5.780	8.20	−5.793	−5.771	0.022	−99.28
TG@CPP	−8631.440	−5.381	5.381	0.73	−6.702	−4.042	2.660	−12.64
TG@N-CPP	−9512.909	−6.168	6.168	15.47	−6.693	−5.618	1.074	−64.72
TG@O-CPP	−10972.705	−6.184	6.184	15.77	−6.178	−6.171	0.006	−99.80

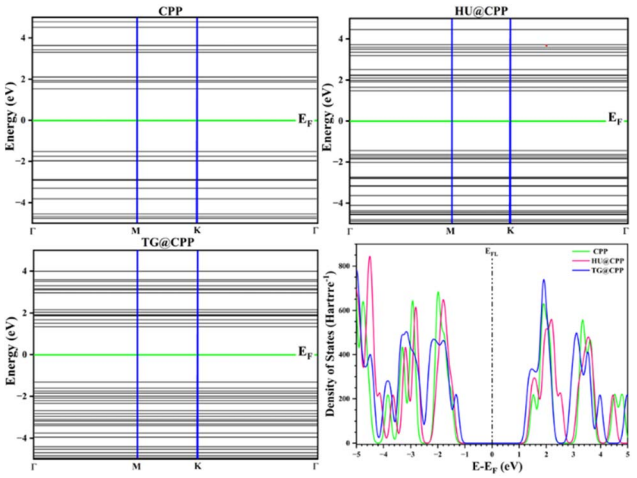

Fig. 3 DOS and band structures of CPP before and after HU and TG molecules adsorption.

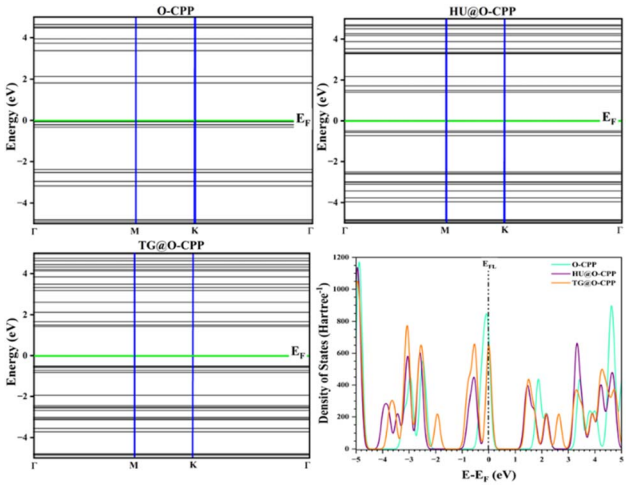

Fig. 5 DOS and band structures of N-CPP before and after HU and TG molecules adsorption.

nearly completely collapsed to 0.02 eV, indicating a significant orbital overlap between the HU frontier levels and the O-CPP host.

The electronic structure was even more significantly impacted by TG adsorption. The gap was moderately reduced to 2.66 eV by TG@CPP, while it was further reduced to 1.07 eV by TG@N-CPP. A remarkable feature of TG@O-CPP was its nearly nonexistent band gap (0.006 eV), which effectively shifted the system toward metallic behavior. The band-structure diagrams plainly demonstrate these trends, as the conduction and valence bands converge near the Fermi level as a result of drug adsorption on doped systems.

The band-gap variations for pristine and drug-loaded CPP frameworks are compared in (Fig. 6). The gaps in pristine CPP and N-CPP were relatively large (approximately 3.0 eV), and the values were only barely perturbed by HU adsorption, indicating a feeble interaction with the host. Conversely, TG resulted in a more substantial reduction, particularly in N-CPP, where the distance decreased to approximately 1.1 eV. The most remarkable effect was observed in O-CPP, where the gap was nearly completely suppressed by both HU and TG adsorption, resulting in near-zero values. These findings confirm the DOS and band-structure analyses (Fig. 3–5) and underscore the critical function of oxygen supplementation in enhancing the electronic response to drug binding.

In general, the combined DOS, band-structure, and HOMO–LUMO analyses indicate that pristine CPP maintains semiconducting characteristics upon drug loading, whereas modified frameworks, particularly O-CPP, undergo significant gap suppression. The potential of doped CPPs as tunable nanocarriers capable of responding sensitively to drug binding is underscored by this behavior, which also emphasizes the role of heteroatom doping in modulating the electronic response.

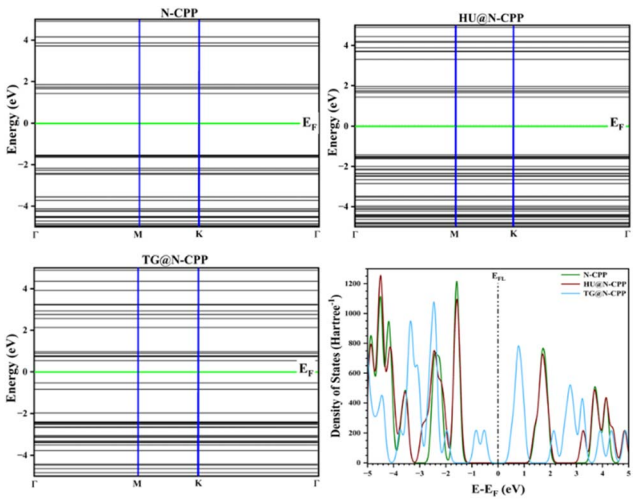

Fig. 4 DOS and band structures of N-CPP before and after HU and TG molecules adsorption.

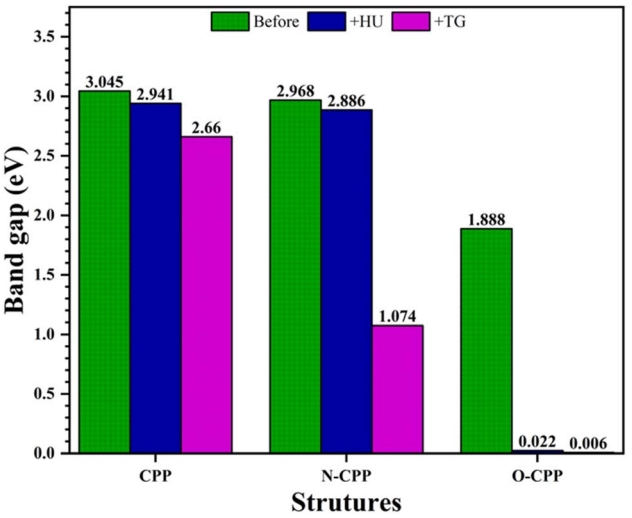

Fig. 6 Band gap modulation in CPP, N-CPP, and O-CPP before and after drug adsorption.

Table 3 The adsorption energy (E_{Ads}), BSSE, and the recovery time for all complex structures

Structure	E_{ads} (s)	BSSE (eV)	$E_{Ads+coor}$ (eV)	$\tau_{300\ K}$ (s)	$\tau_{310\ K}$ (s)
With BSSE					
HU@CPP	−0.801	+0.812	+0.010	$\sim 1.0 \times 10^{-13}$ s	$\sim 1.0 \times 10^{-13}$ s
HU@N-CPP	−0.100	+0.710	+0.609	$\sim 1.0 \times 10^{-13}$ s	$\sim 1.0 \times 10^{-13}$ s
HU@O-CPP	−0.778	+0.746	−0.033	3.6×10^{-13} s	3.4×10^{-13} s
TG@CPP	−1.127	+0.581	−0.547	1.6×10^{-4} s	7.8×10^{-5} s
TG@N-CPP	−0.650	+0.448	−0.202	2.5×10^{-10} s	1.9×10^{-10} s
TG@O-CPP	−1.126	+0.456	−0.671	1.9×10^{-2} s	8.1×10^{-3} s
Without BSSE					
HU@CPP	−0.801	—	−0.801	2.86 s	1.05 s
HU@N-CPP	−0.100	—	−0.100	4.8×10^{-12} s	4.2×10^{-12} s
HU@O-CPP	−0.778	—	−0.778	1.17 s	0.45 s
TG@CPP	−1.127	—	−1.127	8.6×10^{5} s	2.1×10^{5} s
TG@N-CPP	−0.650	—	−0.650	8.3×10^{-3} s	3.7×10^{-3} s
TG@O-CPP	−1.126	—	−1.126	8.2×10^{5} s	2.0×10^{5} s

3.3 Recovery dynamics, charge transfer, and adsorption energetics

The comprehensive comprehension of drug-carrier interactions in CPP-based nanostructures is facilitated by the interplay between adsorption energetics, charge redistribution, and recovery dynamics (Tables 1 and 3). The adsorption energies, which are consistent with physisorption rather than covalent bonding, range from −0.10 to −1.13 eV in the absence of BSSE correction. The binding of HU complexes is comparatively feeble (−0.10 to −0.80 eV), whereas TG binds more firmly, particularly on O-CPP (−1.13 eV). HU@CPP and HU@N-CPP exhibit essentially non-binding behavior, HU@O-CPP exhibits only marginal stability, and TG complexes retain moderate stabilization (−0.20 to −0.67 eV) following BSSE correction. Adsorption intensities diminish significantly. As previously emphasized for drug-nanocarbon systems,[34] the significance of employing BSSE to prevent overestimation of interaction strength is underscored by these corrected values.

The charge-transfer analysis demonstrates a clear distinction between HU and TG. The inherently distinct donor–acceptor character of HU and TG is underscored by the fact that HU donates electrons to the carrier ($\Delta q \approx -0.11$ to −0.18 e) and TG accepts electrons ($\Delta q \approx 0.09$–0.14 e). This opposing behavior is indicative of their intrinsic frontier orbital structures and has been documented in related research on anticancer medications adsorbed onto graphene and carbon nanotubes.[35–37] Oxygen substitution increases the magnitude of Δq as a result of increased polarity, while nitrogen doping promotes directional interactions that more effectively stabilize TG. These effects are amplified by doping. Doped systems are particularly susceptible to drug adsorption due to the synergy of improved charge transfer and stronger binding.

Kinetic insight into the stability of drug binding is provided by recovery times (τ), where recovery time (τ) is frequently employed as a release tendency indicator in theoretical investigations. A shorter τ indicates a more rapid release and simpler desorption, while a longer τ indicates a lengthier residence and stronger retention. In the corrected scenario, the desorption of HU complexes occurs almost instantly ($\sim 10^{-13}$ s), which is consistent with their limited stabilization. In contrast, TG complexes, particularly TG@CPP and TG@O-CPP, exhibit prolonged recovery periods of approximately 0.1 ms and 8–19 ms, respectively. This underscores the critical function of oxygen doping in extending the adsorption process. These millisecond timescales are particularly pertinent for biosensing applications that necessitate rapid response and regeneration.[38] Conversely, the apparent recovery times of TG@CPP and TG@O-CPP are significantly longer when BSSE is disregarded, with desorption times of approximately 10 days and 2 days, respectively, at 300–310 K. Although these values are optimistic upper bounds, they are in close proximity to the therapeutically relevant window for controlled drug release, which is consistent with studies that have reported day-scale retention in nanocarbon-based carriers.[39–41]

When considered collectively, the analysis of adsorption energy, charge transfer, and recovery dynamics establishes a coherent structure-property relationship. HU functions as a weakly binding electron donor, resulting in rapid desorption, whereas TG functions as a stronger-binding electron acceptor with extended residence periods. The most plausible candidate is TG@O-CPP, as oxygen loading improves both adsorption strength and charge transfer. The uncorrected upper-bound scenario implies that TG@O-CPP could also be used in drug-delivery applications with the addition of additional chemical modifications (*e.g.*, pH-sensitive or redox-cleavable linkers), while the corrected data identify this system as highly suitable for biosensing. The broader literature emphasizes the role of heteroatom doping in modulating adsorption energetics and release dynamics in nanocarbon-based systems, which is consistent with these findings.[42–44]

3.4 Modulation of work function

The work function (Φ) is a critical descriptor of surface electronic properties that is directly correlated with electron emission, charge transfer efficiency, and interfacial reactivity. The calculated value of Φ for pristine CPP is 5.34 eV (Table 1), which

agrees with the reported values for conjugated carbon nanohoops and comparable nanocarbon materials.[45–48] The electron-withdrawing nature of nitrogen and the stabilization of the Fermi level were reflected in the increase of the work function to 6.85 eV as a result of nitrogen doping. In addition to nitrogen doping, oxygen doping also increased Φ to 5.87 eV, albeit to a diminished extent, as a result of the introduction of polar oxygen states within the π-framework.

Significant changes in Φ were observed as a result of drug adsorption, which suggests that the interfacial charge was redistributed. HU@CPP and HU@N-CPP exhibited moderate increases in comparison to the pristine carriers, whereas HU@O-CPP exhibited a much greater variation, which was consistent with its nearly nonexistent band gap. The effects of TG complexes were even more pronounced: TG@CPP and TG@N-CPP shifted Φ by 10–15%, while TG@O-CPP exhibited the strongest modulation, with work-function values exceeding 25% change compared to virgin O-CPP. These differences are indicative of the combined impact of orbital overlap and charge-transfer directionality (donor *versus* acceptor behavior), which was previously addressed.

This tunability of Φ is of paramount importance for both sensing and delivery applications. In the field of biosensing, the accuracy of detection is improved by a higher work function, which also enhances surface sensitivity and charge-transfer efficiency.[49–51] Modulation of Φ in drug delivery suggests a responsive interface that can be activated by external stimuli, such as pH or light, to initiate controlled release.[52–54] The dual role of drug adsorption and doping in fine-tuning the electronic landscape of CPP-based carriers is emphasized by the observed trends, which provide a rational pathway to multifunctional nanoplatforms.

3.5 Indexes of global reactivity

To gain a more comprehensive understanding of the stability and reactivity of pristine and functionalized CPP systems, the global reactivity descriptors chemical hardness (η), softness (S), chemical potential (μ), and electrophilicity index (ω) were calculated (Table 4). The conceptual context provided by these descriptors is derived from density functional theory and establishes a connection between chemical reactivity and electronic structure.

Table 4 Global reactivity indices

Structure	IP	EA	S	η	μ	ω
CPP	6.865	3.819	0.328	1.523	5.342	9.370
N-CPP	8.377	5.409	0.337	1.484	6.893	16.006
O-CPP	5.893	4.005	0.530	0.944	4.949	12.970
HU@CPP	6.697	3.756	0.340	1.470	5.227	9.290
HU@N-CPP	8.163	5.277	0.346	1.443	6.720	15.646
HU@O-CPP	5.793	5.771	46.384	0.011	5.782	1550.567
TG@CPP	6.702	4.042	0.376	1.330	5.372	10.850
TG@N-CPP	6.693	5.618	0.931	0.537	6.156	35.265
TG@O-CPP	6.178	6.171	157.429	0.003	6.174	6001.767

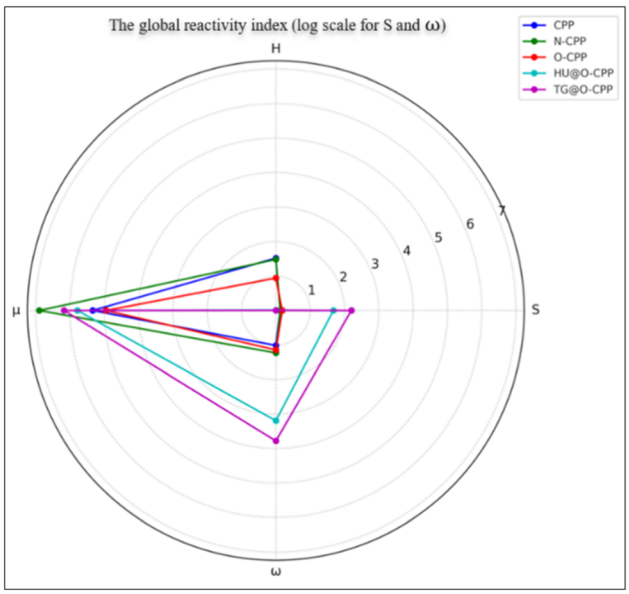

Fig. 7 Global reactivity indices illustrating the effect of doping and drug adsorption on CPP-based frameworks.

The intermediate hardness and low softness of pristine CPP, as illustrated in Fig. 7, are in accordance with its semiconducting nature and relatively wide band gap. Nitrogen supplementation results in a minor decrease in hardness and an increase in suppleness, which is indicative of improved electronic reactivity and polarizability. The more pronounced effect of oxygen supplementation is the reduction of η and the elevation of ω, which indicates a stronger electrophilic nature.

The reactivity indices exhibit substantial fluctuations as a result of drug adsorption. Moderate alterations are observed in HU@O-CPP, with a modest decrease in μ and a small increase in softness, indicating that responsiveness has been enhanced without significant destabilization. In contrast, TG@O-CPP demonstrates the most significant alterations: a significant increase in ω and a decrease in hardness, which emphasizes its enhanced susceptibility to charge transfer and amplified electrophilic behavior. The charge-transfer analysis discussed in Section 3.3, which identified TG as a stronger electron acceptor, is corroborated by these results.

The global reactivity profile is substantially influenced by doping and drug adsorption, as evidenced by the radar chart (Fig. 7), which offers a comparative overview of these trends. TG@O-CPP is a prospective candidate for applications that require controlled reactivity and electronic responsiveness, as it possesses high electrophilicity and reduced hardness, which may facilitate robust interactions with biomolecular targets.

3.6 Structure-properties relationship

The established structure-property correlations reveal that the geometric adaptability of pristine and doped CPP frameworks directly governs their electronic response and adsorption performance. Localized distortions induced by nitrogen and oxygen substitution not only preserve the intrinsic backbone

stability but also redistribute the π-electron density, creating preferential adsorption sites. This structural modification results in systematically shorter drug-carrier contact distances, which are directly correlated with stronger adsorption energies and enhanced charge transfer, particularly in TG-loaded systems. The narrowing of the band gap in doped structures, most notably in O-CPP, underscores how subtle atomic substitutions can amplify reactivity and induce metallic-like behavior upon drug binding.

Collectively, these observations confirm that structural perturbations at the molecular level translate into tunable electronic properties and controlled drug-carrier interactions, thereby establishing a clear structure-property relationship that underpins the multifunctional potential of CPP-based nanoplatforms. As evidenced by the optimized geometries (Fig. 1 and 2) and interatomic distances summarized in Table 1, the introduction of nitrogen and oxygen dopants induced localized distortions within the CPP nanohoops, which facilitated closer drug-carrier contacts. These geometric perturbations correlate directly with the adsorption-energy hierarchy in Table 3, where doped frameworks consistently exhibit stronger binding relative to pristine CPP.

For instance, TG@O-CPP exhibits both the shortest interaction distances (∼1.96 Å) and the most negative corrected adsorption energy, highlighting the structural origin of its enhanced stabilization. This closer binding also manifests electronically, as shown in the DOS and band-structure analyses (Fig. 3–6), where doped systems exhibit a pronounced suppression of the energy gap, with TG@O-CPP reaching near-metallic behavior (0.006 eV, Table 2). The global reactivity descriptors (Table 4) further validate this relationship, as oxygen substitution simultaneously reduces chemical hardness and increases electrophilicity, thereby amplifying the carrier's susceptibility to charge transfer. Together, these results establish a coherent structure-property relationship: dopant-induced geometric distortions directly modulate adsorption strength, charge redistribution, and band-gap suppression, ultimately dictating the drug-carrier interaction dynamics. In our calculations the incorporation of N and O into the CPP backbone shortens the drug-carrier contact (HU: 2.06–2.23 Å; TG: 1.92–2.26 Å) and shifts the direction of charge transfer (HU donates $\approx -0.11 \rightarrow -0.18$ e; TG accepts $\approx +0.09 \rightarrow +0.14$ e), producing an adsorption-energy hierarchy from weak HU binding (uncorrected $-0.10 \rightarrow -0.80$ eV; BSSE-corrected $\approx 0 \rightarrow -0.78$ eV) to substantially stronger TG binding (uncorrected down to −1.13 eV; corrected values remain more stabilizing than HU). These trends correlate with large electronic responses: TG@O-CPP shows near-metallic gap quenching (∼0.006 eV) whereas HU perturbs the host gap only slightly.

In summary, the structure-property relationship in CPP-based frameworks is dictated by dopant-induced geometric perturbations that redistribute electronic density and create preferential adsorption sites. Nitrogen and oxygen substitution systematically shorten drug-carrier distances, enhance charge transfer, and intensify band-gap suppression, particularly in TG@O-CPP, which approaches metallic behavior. HU acts as a weak electron donor with rapid desorption, whereas TG functions as a robust acceptor with stronger binding and extended residence times. These results confirm that local structural modifications translate into tunable electronic properties and controlled drug-carrier interactions, positioning doped CPPs as versatile candidates for both biosensing and targeted drug delivery applications.[29,55,56]

In the context of biosensing, CPP-based systems have the potential to function as sensitive platforms for the detection of biologically relevant molecules through adsorption-induced electronic modulation. Anticancer pharmaceuticals and nucleobase derivatives, as well as minor biomolecules like urea, glucose, dopamine, uric acid, and amino acids, are potential target analytes. The fundamental sensing mechanism in carbon-based nanomaterials is the measurable variations in key electronic parameters, such as band gap, density of states, charge transfer, and work function, that can be induced by the adsorption of such analytes.[57,58] From a cellular standpoint, the electronic and adsorption characteristics that were identified in this study offer a preliminary understanding of the potential interactions between doped CPP systems and biological environments. Key parameters that influence cellular uptake, intracellular stability, and drug-carrier residence time include enhanced charge transfer, tunable work function, and controllable adsorption strength. It is possible that intracellular drug retention may be favored by moderate binding energies and finite recovery periods, while subsequent release is still possible. While the current DFT investigation does not encompass explicit cellular modeling, these findings provide a theoretical framework for future *in vitro* and *in vivo* studies of CPP-based nanocarriers.

4. Conclusion

The present study thoroughly investigated the structural, electronic, and adsorption characteristics of pristine and doped cycloparaphenylene (CPP, N-CPP, and O-CPP) in relation to their interactions with the anticancer agents' hydroxyurea (HU) and thioguanine (TG). Geometry optimizations demonstrated that all carriers maintain their inherent stability, whereas doping induces localized distortions that augment reactivity and establish preferred binding sites.

Electronic investigations indicated that doping considerably reduces the band gap and promotes charge redistribution, especially in O-CPP systems. HU was recognized as a weakly interacting electron donor, resulting in very slight perturbations, whereas TG functioned as a more potent electron acceptor, causing significant band gap quenching and near-metallic behavior in TG@O-CPP. Global reactivity indices confirmed these findings, demonstrating increased electrophilicity and reduced hardness upon TG adsorption, particularly in the oxygen-doped framework.

The energetics and kinetics of adsorption further emphasized the differing behaviors of the two pharmaceuticals. HU complexes had minimal adsorption energies, negative charge transfer, and very quick recovery periods, indicative of swift release and inadequate retention. TG, in contrast, exhibited enhanced adsorption, positive charge transfer, and extended

recovery durations, especially in TG@O-CPP, where the synergistic effects of doping and drug binding produced the most stable and responsive complex.

The findings together indicate that doping effectively adjusts the adsorption strength, electrical characteristics, and reactivity of CPP-based nanocarriers. Of all the systems analyzed, TG@O-CPP stands out as the most promising contender, exhibiting superior binding, robust charge transfer, and adjustable electrical responsiveness. These results provide significant insights into the methodical design of cycloparaphenylene-based nanostructures for applications in biosensing and drug delivery, necessitating careful regulation of drug-carrier interactions.

The proposed computational framework is not confined to hydroxyurea and thioguanine and may be easily expanded to include additional pharmacological substances. Specifically, tiny anticancer agents such 5-fluorouracil, methotrexate, doxorubicin, cisplatin derivatives, and nucleobase analogues are promising prospects for further research. This adaptability underscores the promise of doped CPP nanostructures as flexible platforms for evaluating drug-carrier interactions before experimental validation.

Author contributions

All authors contributed to the conception and design of the study. Noora B. Shwayyea, Alaa M. Khudhair and Fouad N. Ajeel performed material preparation, computations, data collection and analysis and Ali Ben Ahmed supervised this study. All authors discussed the results and contributed to reading and approving the final manuscript.

Conflicts of interest

There are no conflicts to declare.

Data availability

The data (all optimized structures CPP, N-CPP, O-CPP, HU@CPP, HU@N-CPP, HU@O-CPP, TG@CPP, TG@N-CPP and TG@O-CPP) supporting this article have been included as part of the supplementary information (SI). Supplementary information is available. See DOI: https://doi.org/10.1039/d5ra09445c.

References

1 J. Ferlay, M. Ervik, F. Lam, M. Colombet, L. Mery and M. Piñeros, *Global Cancer Observatory: Cancer Today*, International Agency for Research on Cancer, Lyon, 2020, https://gco.iarc.fr/today.
2 D. Hanahan and R. A. Weinberg, Hallmarks of Cancer: The Next Generation, *Cell*, 2011, **144**, 646–674.
3 F. Bray, J. Ferlay, I. Soerjomataram, R. L. Siegel, L. A. Torre and A. Jemal, Global cancer statistics 2018: GLOBOCAN estimates of incidence and mortality worldwide for 36 cancers in 185 countries, *Ca-Cancer J. Clin.*, 2018, **68**, 394–424.
4 C. Holohan, S. Van Schaeybroeck, D. B. Longley and P. G. Johnston, Cancer drug resistance: an evolving paradigm, *Nat. Rev. Cancer*, 2013, **13**, 714–726.
5 D. Peer, J. M. Karp, S. Hong, O. C. Farokhzad, R. Margalit and R. Langer, Nanocarriers as an emerging platform for cancer therapy, *Nat. Nanotechnol.*, 2007, **2**, 751–760.
6 J. Shi, A. R. Votruba, O. C. Farokhzad and R. Langer, Nanotechnology in Drug Delivery and Tissue Engineering: From Discovery to Applications, *Nano Lett.*, 2010, **10**, 3223–3230.
7 S. M. Moghimi, A. C. Hunter and J. C. Murray, Nanomedicine: current status and future prospects, *FASEB J.*, 2005, **19**, 311–330.
8 E. Blanco, H. Shen and M. Ferrari, Principles of nanoparticle design for overcoming biological barriers to drug delivery, *Nat. Biotechnol.*, 2015, **33**, 941–951.
9 R. Jasti, J. Bhattacharjee, J. B. Neaton and C. R. Bertozzi, Synthesis, Characterization, and Theory of [9]-, [12]-, and [18]Cycloparaphenylene: Carbon Nanohoop Structures, *J. Am. Chem. Soc.*, 2008, **130**, 17646–17647.
10 S. Yamago, E. Kayahara and T. Iwamoto, Organoplatinum-Mediated Synthesis of Cyclic π-Conjugated Molecules: Towards a New Era of Three-Dimensional Aromatic Compounds, *Chem. Rec.*, 2014, **14**, 84–100.
11 Y. Segawa, A. Yagi, K. Matsui and K. Itami, Design and Synthesis of Carbon Nanotube Segments, *Angew. Chem., Int. Ed.*, 2016, **55**, 5136–5158.
12 G. Bottari, G. de la Torre, D. M. Guldi and T. Torres, Covalent and Noncovalent Phthalocyanine-Carbon Nanostructure Systems: Synthesis, Photoinduced Electron Transfer, and Application to Molecular Photovoltaics, *Chem. Rev.*, 2010, **110**, 6768–6816.
13 A. Mahor, P. P. Singh, P. Bharadwaj, N. Sharma, S. Yadav, J. M. Rosenholm and K. K. Bansal, Carbon-Based Nanomaterials for Delivery of Biologicals and Therapeutics: A Cutting-Edge Technology, *C*, 2021, **7**, 19.
14 S. Charache, M. L. Terrin, R. D. Moore, G. J. Dover, F. B. Barton, S. V. Eckert, R. P. McMahon and D. R. Bonds, Effect of Hydroxyurea on the Frequency of Painful Crises in Sickle Cell Anemia, *N. Engl. J. Med.*, 1995, **332**, 1317–1322.
15 J. W. Yarbro, Mechanism of action of hydroxyurea, *Semin. Oncol.*, 1992, **19**, 1–10.
16 L. K. G. I. Teitelbaum, T. H. K. D. A. Levin, G. R. B. M. A. Jones and N. M. S. K. S. Lundin, *Renal Pharmacotherapy*, Springer New York, New York, NY, 2013.
17 L. Lennard, The clinical pharmacology of 6-mercaptopurine, *Eur. J. Clin. Pharmacol.*, 1992, **43**, 329–339.
18 G. B. Elion, The Purine Path to Chemotherapy, *Science*, 1989, **244**, 41–47.
19 A. Teml, E. Schaeffeler, K. R. Herrlinger, U. Klotz and M. Schwab, Thiopurine Treatment in Inflammatory Bowel Disease, *Clin. Pharmacokinet.*, 2007, **46**, 187–208.
20 M. Ferrari, Cancer nanotechnology: opportunities and challenges, *Nat. Rev. Cancer*, 2005, **5**, 161–171.

21 G. Storm, F. J. Koppenhagen, A. L. M. Heeremans, M. H. Vingerhoeds, M. C. Woodle and D. J. A. Crommelin, Liposomal Delivery of Peptides and Proteins, *J. Liposome Res.*, 1995, **5**, 481–489.
22 M. T. Luiz, J. A. P. Dutra, J. S. R. Viegas, J. T. C. de Araújo, A. G. Tavares Junior and M. Chorilli, Hybrid Magnetic Lipid-Based Nanoparticles for Cancer Therapy, *Pharmaceutics*, 2023, **15**, 1–22.
23 M. Fujitsuka and T. Majima, Charge transfer dynamics in DNA revealed by time-resolved spectroscopy, *Chem. Sci.*, 2017, **8**, 1752–1762.
24 R. M. Pinto, C. L. Seabra, M. De Jonge, M. C. L. Martins, P. Van Dijck, S. Reis and C. Nunes, Antibiofilm Combinatory Strategy: Moxifloxacin-Loaded Nanosystems and Encapsulated N-Acetyl-L-Cysteine, *Pharmaceutics*, 2022, **14**, 2294.
25 H. Zuo, J. Tao, M. Wang, X. Xie and M. Sun, A novel immunochemotherapy based on immunogenicity-activated and immunosuppression-reversed biomimetic nanoparticles, *RSC Adv.*, 2022, **12**, 28104–28112.
26 S. Smidstrup, T. Markussen, P. Vancraeyveld, J. Wellendorff, J. Schneider, T. Gunst, B. Verstichel, D. Stradi, P. A. Khomyakov, U. G. Vej-Hansen, M.-E. Lee, S. T. Chill, F. Rasmussen, G. Penazzi, F. Corsetti, A. Ojanperä, K. Jensen, M. L. N. Palsgaard, U. Martinez, A. Blom, M. Brandbyge and K. Stokbro, QuantumATK: an integrated platform of electronic and atomic-scale modelling tools, *J. Phys. Condens. Matter*, 2020, **32**, 015901.
27 S. Grimme, A. Hansen, J. G. Brandenburg and C. Bannwarth, Dispersion-Corrected Mean-Field Electronic Structure Methods, *Chem. Rev.*, 2016, **116**, 5105–5154.
28 A. García, N. Papior, A. Akhtar, E. Artacho, V. Blum, E. Bosoni, P. Brandimarte, M. Brandbyge, J. I. Cerdá, F. Corsetti, R. Cuadrado, V. Dikan, J. Ferrer, J. Gale, P. García-Fernández, V. M. García-Suárez, S. García, G. Huhs, S. Illera, R. Korytár, P. Koval, I. Lebedeva, L. Lin, P. López-Tarifa, S. G. Mayo, S. Mohr, P. Ordejón, A. Postnikov, Y. Pouillon, M. Pruneda, R. Robles, D. Sánchez-Portal, J. M. Soler, R. Ullah, V. W. Yu and J. Junquera, Siesta : Recent developments and applications, *J. Chem. Phys.*, 2020, **152**(20), 204108.
29 A. M. Khudhair, A. Ben Ahmed and F. N. Ajeel, Computational Investigation of 6-Thioguanine Adsorption on Armchair Graphene Nanoribbons for Targeted Drug Delivery: Orientation-Dependent Stability, Electronic Structure, and Delivery Efficiency, *J. Phys. Chem. C*, 2025, **129**, 16593–16603.
30 A. M. Khudhair, A. Ben Ahmed, F. N. Ajeel and M. H. Mohammed, Theoretical investigation on the therapeutic applications of C2B and C2O as targeted drug delivery systems for hydroxyurea and 6-thioguanine in cancer treatment, *Nano-Struct. Nano-Objects*, 2024, **38**, 101135.
31 A. M. Khudhair and A. Ben Ahmed, The Present and Doped Bilayer Circumcoronene and Bilayer BN Circumcoronene as Carriers for Hydroxyurea Anticancer Drug Delivery, *Bionanoscience*, 2024, **14**, 2976–2992.
32 A. M. Khudhair and A. Ben Ahmed, First investigation survey on the pristine C3N3 and B3O3 monolayer as a promising vehicle for delivery of 5-fluorouracil and cisplatin anticancer drugs, *Chin. J. Phys.*, 2025, **95**, 674–684.
33 A. M. Khudhair, I. Dhouib, A. Ben Ahmed, F. N. Ajeel and B. Khemakhem, DFT-based insights into cisplatin drug adsorption on transition metal dichalcogenides: toward targeted drug delivery systems, *Chin. J. Phys.*, 2025, **97**, 827–838.
34 S. Shukla, J. Jakowski, S. Kadian and R. J. Narayan, Computational approaches to delivery of anticancer drugs with multidimensional nanomaterials, *Comput. Struct. Biotechnol. J.*, 2023, **21**, 4149–4158.
35 S. Alfei, C. Reggio and G. Zuccari, Carbon Nanotubes as Excellent Adjuvants for Anticancer Therapeutics and Cancer Diagnosis: A Plethora of Laboratory Studies Versus Few Clinical Trials, *Cells*, 2025, **14**, 1052.
36 L. R. M. de Andrade, L. N. Andrade, J. O. Bahú, V. O. Cárdenas Concha, A. T. Machado, D. S. Pires, R. Santos, T. F. M. Cardoso, J. C. Cardoso, R. L. C. Albuquerque-Junior, P. Severino and E. B. Souto, Biomedical applications of carbon nanotubes: A systematic review of data and clinical trials, *J. Drug Deliv. Sci. Technol.*, 2024, **99**, 105932.
37 K. Sumetpipat, D. Baowan and P. Tiangtrong, Mathematical modeling and optimization technique of anticancer antibiotic adsorption onto carbon nanocarriers, *Sci. Rep.*, 2024, **14**, 11988.
38 S. Yücer, B. Sarac and F. Ciftci, Tissue engineering and biosensing applications of carbon-based nanomaterials, *Adv. Biomed. Eng.*, 2025, **9**, 100145.
39 J. K. Patra, G. Das, L. F. Fraceto, E. V. R. Campos, M. del P. Rodriguez-Torres, L. S. Acosta-Torres, L. A. Diaz-Torres, R. Grillo, M. K. Swamy, S. Sharma, S. Habtemariam and H.-S. Shin, Nano based drug delivery systems: recent developments and future prospects, *J. Nanobiotechnol.*, 2018, **16**, 71.
40 P. K. Jiwanti, B. Y. Wardhana, L. G. Sutanto, D. M. M. Dewi, I. Z. D. Putri and I. N. I. Savitri, Recent Development of Nano-Carbon Material in Pharmaceutical Application: A Review, *Molecules*, 2022, **27**, 7578.
41 M. Abd Elkodous, S. O. Olojede, M. Morsi and G. S. El-Sayyad, Nanomaterial-based drug delivery systems as promising carriers for patients with COVID-19, *RSC Adv.*, 2021, **11**, 26463–26480.
42 J. Mall, N. Naseem, M. F. Haider, M. A. Rahman, S. Khan and S. N. Siddiqui, Nanostructured lipid carriers as a drug delivery system: A comprehensive review with therapeutic applications, *Intell. Pharm.*, 2025, **3**, 243–255.
43 A. N. Kuskov, E. V. Kukovyakina and E. N. Krasnoselskaya, Nanotechnology-Based Drug Delivery Systems, *Pharmaceutics*, 2025, **17**, 817.
44 Y. Jia, Z. Zhao, L. Chen, Y. Liu and B. Zhu, Carbon Nanotube-Based Drug Delivery System Increases Drug Content and Promotes Immune Response in Mandarin Fish, *Fishes*, 2025, **10**, 92.

45 K. Kovida, J. Malinčík and T. Šolomek, Effect of π-Electron Conjugation on the Chiroptical Properties of Helicene Carbon Nanohoops, *Helv. Chim. Acta*, 2025, **108**, e202400166.
46 S. Y. R. Rahchamandi, E. Mirhadi, F. Gheybi, A. Kazemi-Beydokhti, M. R. Jaafari, E. Mostafavi, P. Kesharwani, A. Sahebkar and S. H. Alavizadeh, Engineering carbon-based nanomaterials for the delivery of platinum compounds: An innovative cancer disarming frontier, *Environ. Res.*, 2024, **262**, 119933.
47 N. Jayaprakash, K. Elumalai, S. Manickam, G. Bakthavatchalam and P. Tamilselvan, Carbon nanomaterials: Revolutionizing biomedical applications with promising potential, *Nano Mater. Sci.*, 2024, 1–16.
48 S. D. Hettiarachchi, R. M. Graham, K. J. Mintz, Y. Zhou, S. Vanni, Z. Peng and R. M. Leblanc, Triple conjugated carbon dots as a nano-drug delivery model for glioblastoma brain tumors, *Nanoscale*, 2019, **11**, 6192–6205.
49 W. Yang, K. Yan, Y. Feng and X. Zhao, Charge reversible hyaluronic acid-based drug delivery system with pH-responsive dissociation for enhanced drug delivery, *Eur. J. Pharm. Biopharm.*, 2024, **205**, 114560.
50 R. Zhao, Y. Zhu, Z. Tang, H. Lin and J. Shi, Modulation of electron transfer properties in two-dimensional nanomaterials for enhanced therapeutic efficacy, *Nano Today*, 2025, **65**, 102880.
51 M. Gorohovs and Y. Dekhtyar, Surface Functionalization of Nanoparticles for Enhanced Electrostatic Adsorption of Biomolecules, *Molecules*, 2025, **30**, 3206.
52 H. Ding, P. Tan, S. Fu, X. Tian, H. Zhang, X. Ma, Z. Gu and K. Luo, Preparation and application of pH-responsive drug delivery systems, *J. Contr. Release*, 2022, **348**, 206–238.
53 S. Adepu and S. Ramakrishna, Controlled Drug Delivery Systems: Current Status and Future Directions, *Molecules*, 2021, **26**, 5905.
54 A. Z. Juthi, F. Li, B. Wang, M. M. Alam, M. E. Talukder and B. Qiu, pH-Responsive Super-Porous Hybrid Hydrogels for Gastroretentive Controlled-Release Drug Delivery, *Pharmaceutics*, 2023, **15**, 816.
55 R. Rahimi, M. Solimannejad and M. Soleimannejad, Two-dimensionalcovalent triazine frameworks as superior nanocarriers for the delivery of thioguanine anti-cancer drugs: a periodic DFT study, *New J. Chem.*, 2022, **46**, 15635–15644.
56 M. H. Opi, T. Ahmed, M. R. Swarna, A. A. Piya and S. U. D. Shamim, Assessment of the drug delivery potential of graphene, boron nitride and their in-plane doped structures for hydroxyurea anti-cancer drug via DFT study, *Nanoscale Adv.*, 2024, **6**, 5042–5054.
57 A. K. Geim and K. S. Novoselov, The rise of graphene, *Nat. Mater.*, 2007, **6**, 183–191.
58 Z. Wang, R. C. Beier and J. Shen, Immunoassays for the detection of macrocyclic lactones in food matrices – A review, *Trac. Trends Anal. Chem.*, 2017, **92**, 42–61.